Antibacterial and Antifungal of β-sitosterol Isolated from Hydroid *Aglaophenia cupressina* Lamoureoux Against *Xanthomonas campestris* and *Fusarium oxysporum*

Eva Johannes[1]*, Baso Manguntungi[2], Mustika Tuwo[1], Magdalena Litaay[1], Apon Zaenal Mustopa[3], Leggina Rezzy Vanggy[4]

[1]Department of Biology, Faculty of Mathematic and Natural Science Faculty, Hasanuddin University
Jl. Perintis Kemerdekaan KM 10. Tamalanrea Makassar, Sulawesi Selatan 90245 Indonesia,
[2]Department of Biotechnology, Universitas Sulawesi Barat
Jl. Poros Majene - Mamuju Baurung Sulawesi Barat 91412 Indonesia
[3]Research Center for Biotechnology, National Research and Innovation Agency
Jl. Raya Jakarta-Bogor Km. 46, Cibinong Jawa Barat 16911 Indonesia
[4]Sekolah Ilmu dan Teknologi Hayati, Institut Teknologi Bandung
Jl. Ganesa 10, Bandung Jawa Barat 40132 Indonesia
Email: evayohannes@unhas.ac.id

Abstract

This study aimed to isolate and characterize β-sitosterol from the marine hydroid Aglaophenia cupressina Lamoureoux and evaluate its antibacterial and antifungal activities against Xanthomonas campestris and Fusarium oxysporum. β-Sitosterol was extracted, purified, and identified using spectroscopic techniques, including infrared and nuclear magnetic resonance spectroscopy. Antimicrobial activity was assessed through agar diffusion method to determine its inhibitory effects on bacterial and fungal growth at varying concentrations. β-sitosterol is a crystalline compound, with a melting point of 138-139 °C, consistent with the reported range for pure β-sitosterol, indicating high purity. Infrared (IR) spectroscopy revealed key functional groups, including a hydroxyl group at 3433 cm^{-1}, C-O stretching at 1050 cm^{-1}, and aliphatic hydrocarbon chain vibrations at 2956, 2938, and 2869 cm^{-1}. The C=C stretching at 1634 cm^{-1} and C-H bending at 1465 cm^{-1} confirmed its unsaturated sterol structure. ^{1}H NMR spectroscopy further confirmed the structure with characteristic methyl and olefinic proton signals. The antibacterial activity of β-sitosterol against Xanthomonas campestris showed a concentration- and time-dependent effect, with the highest efficacy observed at 60 ppm, demonstrating potential as a natural antibacterial agent. Additionally, its antifungal activity against Fusarium oxysporum revealed both fungistatic and fungicidal effects, with lower concentrations exhibiting fungistatic behavior and higher concentrations displaying fungicidal activity, thereby offering versatility for both fungal inhibition and eradication. This dual action, combined with its well-characterized molecular structure, positions β-sitosterol as a promising candidate for further development as an antimicrobial compound. The findings underscore the accuracy of the identification process and highlight β-sitosterol's potential in pharmaceutical and agricultural applications, particularly in combating bacterial and fungal infections.

Keywords: *β-sitosterol, Aglaophenia cupressina Lamoureoux, Antibacterial, Antifungal.*

Introduction

Wilt rot disease is a major threat to vegetable crops, particularly mustard greens (*Brassica juncea* L.), due to its detrimental impact on yield and quality. This disease is caused by both the bacterium *Xanthomonas campestris* and the fungus *Fusarium oxysporum*, which infect plants through different mechanisms but ultimately lead to severe plant deterioration (Meena *et al*., 2021). Given the high economic losses associated with wilt rot disease, understanding its causative agents and developing effective control strategies are critical for sustainable agricultural production. *X. campestris* is a Gram-negative bacterium characterized by its round, yellow, mucoid, convex, and shiny colonies (Chen *et al*., 2022). The bacterium enters plant tissues through water pores (hydathodes, emissaria) located at the ends of vascular bundles on leaf edges, leading to progressive leaf fall, dryness, and eventual wet rot, accompanied by an unpleasant odor. Meanwhile, *F. oxysporum* colonizes the plant's vascular system and basal tissues, forming a dense network of white mycelial threads that contribute to bark decay (de Lamo and Takken, 2020). This fungal pathogen is highly persistent in soil, capable of surviving in the form of mycelium, microconidia, macroconidia, and chlamydospores, even in the

*) Corresponding author

https://ejournal.undip.ac.id/index.php/ijms
DOI: 10.14710/ik.ijms.30.2.192-202
Received : 03-01-2025
Accepted : 08-03-2025

absence of a host plant (Hassan, 2020; Ullah *et al*., 2021; Gwinn *et al*., 2022). Infected plants exhibit yellowing of leaf veins, followed by progressive wilting and eventual plant death (Soleha *et al*., 2022). Under favorable environmental conditions, *F. oxysporum* can cause losses of up to 80%, making its management particularly challenging (Sampaio *et al*., 2020).

To mitigate the adverse effects of wilt rot disease, farmers have traditionally relied on synthetic pesticides. However, the indiscriminate and excessive use of chemical pesticides has led to increasing concerns over food safety, environmental contamination, and the emergence of resistant pathogen strains (Hassaan and El Nemr, 2020; Naidu *et al*., 2021). Studies have shown that prolonged application of fungicides in postharvest treatment has contributed to pathogen resistance, raising public awareness of the risks associated with chemical-based disease management (Zubrod *et al*., 2019; Steinberg and Gurr, 2020). As a result, there is a growing need for safer and more sustainable alternatives to control wilt rot disease effectively. One promising approach is the use of biological control methods, which leverage natural bioactive compounds to suppress plant pathogens. Postharvest pathogen management strategies aim to minimize disease incidence, reduce inoculum presence, and eradicate infections to extend the shelf life of vegetables and fruits (Morales-Cedeño *et al*., 2020). In this context, recent research has focused on marine-derived bioactive compounds due to their rich biodiversity and potential antimicrobial properties (Rahim *et al*., 2021).

Among these bioactive compounds, β-sitosterol, a naturally occurring phytosterol, has gained attention for its potent antimicrobial and antifungal properties. Isolated from the marine hydroid *A. cupressina* L., β-sitosterol has been reported to exhibit significant inhibitory effects against *X. campestris* and *F. oxysporum*, two major phytopathogens responsible for causing wilt rot disease in economically important crops. The antimicrobial mechanism of β-sitosterol is linked to its ability to disrupt the structural integrity of microbial cell membranes, leading to increased permeability, leakage of intracellular components, and eventual cell lysis. Additionally, β-sitosterol is believed to interfere with key metabolic pathways by inhibiting ergosterol biosynthesis in fungal pathogens, thereby impairing membrane fluidity and function. The efficacy of β-sitosterol against these pathogens highlights its potential as a biopesticide that could mitigate the negative consequences of synthetic fungicide overuse, such as pathogen resistance and environmental contamination. Given its natural origin and broad-spectrum activity, β-sitosterol represents a promising candidate for integration into sustainable plant disease management programs, aligning with the global push toward eco-friendly agricultural practices (Moosavi *et al*., 2020; Luhata *et al*., 2021; Anwar *et al*., 2022). Further research into the formulation, stability, and application methods of β-sitosterol-based treatments could enhance its practical utility in commercial agriculture, offering a viable alternative to conventional chemical pesticides.

Materials and Methods

Extraction, partition, and isolation of β-sitosterol compound

Initially, Hydroid *A. cupressina* L. was cleaned from the substrate and washed with water until clean. Maceration was performed three times with methanol for 24 h 3 times, followed by filtration and evaporation to obtain thick macerate. Furthermore, the liquid-liquid partition (1:1) with n-hexane was performed where the filtrate layer was evaporated to obtain a thick extract and pure compounds. This process was continued in the vacuum chromatography and press chromatography column. Subsequently, analysis was carried out by thin-layer chromatography and melting point measurements compared to sample of β-sitosterol compounds (Johannes *et al*., 2013). Structural analysis was performed using IR and NMR spectrophotometer at 500.1 MHz (^{1}H) and 125.7 MHz (^{13}C). The structural characterization of β-sitosterol was performed using infrared (IR) and nuclear magnetic resonance (NMR) spectroscopy. IR spectra were recorded using a Fourier Transform Infrared Spectrophotometer (FTIR) in the range of 4000-400 cm^{-1} to identify functional groups present in the compound. The spectra were analyzed based on characteristic absorption peaks corresponding to various functional groups. NMR analysis was conducted using a high-resolution NMR spectrometer at 500.1 MHz for proton (^{1}H) and 125.7 MHz for carbon (^{13}C) nuclei. ^{1}H-NMR and ^{13}C-NMR spectra were recorded in deuterated solvents, with chemical shifts (δ) reported in parts per million (ppm) relative to tetramethylsilane (TMS) as an internal standard. The ^{1}H-NMR spectrum provided insights into the hydrogen environments within the molecule, including signal multiplicity, coupling constants, and chemical shift values. The ^{13}C-NMR spectrum revealed the carbon skeleton, enabling the identification of different carbon types (*e.g*., primary, secondary, tertiary, and quaternary carbons). Additionally, two-dimensional NMR techniques such as heteronuclear single quantum coherence (HSQC) and heteronuclear multiple bond correlation (HMBC) were employed to elucidate connectivity between carbon and hydrogen atoms, confirming the structural integrity of β-sitosterol (Uttu *et al*., 2023; Gomathi *et al*., 2024).

Antibacterial activity of β-sitosterol compound

Antibacterial activity was carried out on *X. campestris* InaCC B1449 using the agar diffusion method. Muller Hinton Agar (MHA) medium was poured into a petri dish aseptically and 10 mL of MHA containing the tested bacterial suspension was poured into a petri dish. The bacterial suspension was adjusted to an OD_{600} of 0.8–1.0, and 75 µL of this suspension was added to the medium before solidification. The reservoir was removed to form a well for the test solution. β-Sitosterol solution (50 µL) at three different concentrations (20, 40, and 60 ppm) was added to each well, carried out in duplicate, and then incubated at 37^{O}C for 24 and 48 h. Ciprofloxacin (5 µg) and distilled water were used as positive and negative controls, respectively. Observations were made by measuring the diameter of the inhibition of bacterial growth around the wells using a caliper.

Antifungal activity of β-sitosterol compound

The antifungal activity was performed on the test fungus *F. oxysporum* InaCC F641 using the agar diffusion method. Sabouraud dextrose agar (SDA) medium was aseptically poured into a petri dish and allowed to solidify as a base layer or "based layer." A total of 1 mL of each test mushroom suspension was added to 10 mL of SDA medium, homogenized, and poured over the base layer, and semi-solid was left as the seed layer. Subsequently, five trays were placed with an inner diameter of 6 mm, an outer diameter of 8 mm, and a height of 10 mm at 2–3 cm from the edge of a petri dish and left at room temperature. β-Sitosterol solution (50 µL) at three different concentrations (20, 40, and 60 ppm) was added to each well, carried out in duplicate, and incubated at 37^{O}C for 48 h and 72 h. Ketoconazole at a concentration of 2% was applied as a positive control and negative control using distilled water. Observations were made by measuring the diameter of inhibition of fungus growth around the enclosure using a caliper.

SEM morphology analysis of β-sitosterol effect against cell damage of Xanthomonas campestris InaCC B1449 and Fusarium oxysporum InaCC F641

Analysis of damage to cell morphology was carried out to determine changes in cell morphology and structure caused by β-sitosterol in *X. campestris* InaCC B1449 and *F. oxysporum* InaCC F641. Changes in the cell appearance and wall thickness were also observed by SEM. The bacterium and fungus cell suspensions treated with β-sitosterol (60 ppm) were incubated for 24 h in a shaker incubator at 150 rpm and 37^{O}C. This was followed by centrifugation at 3,500 rpm for 15 min, the pellet was fixed with 2.5% glutaraldehyde (0.1 M sodium cacodylate buffer pH 7.2) and allowed to stand for 1.5 h. The sample obtained was washed with cacodilat buffer (0.05M, pH 7.2) for 20 min. Cell was fixed with 1% osmium tetraoxide in 0.05% cacodylate buffer (pH 7.2) for 1-2 min, washed with ddH_2O for 2 min, and hydrated with ethanol at various concentrations (25, 50, 75, and 100%) for 10 min each. The sample was passed through a 0.2 µm membrane, glued to aluminum stubs, and coated with gold through a vacuum process (6-7 Pa) for 20 min. Further observation was carried out using a Scanning Electron Microscope (SEM, JEOL 5310) at 3000X magnification.

Data analysis

The data was tested using one-way Analysis of variance (ANOVA), and IBM SPSS 25 with a 5% confidence interval.

Result and Discussion

Identification of β-sitosterol compound

β-sitosterol compound was in the form of white (clear) crystals with a melting point of 138-139^{O}C. The IR spectrum (KBr) showed absorption at 3433 cm^{-1}, suggesting the presence of hydroxyl groups supported by peak at 1050 cm^{-1} which represented C-O. Absorption at 2956, 2938, and 2869 cm^{-1} were obtained from methyl and methylene, while 1634 cm^{-1} came from C=C stretching, showing the presence of olefin groups, and C-H bending appeared at 1465 cm^{-1}. The IR spectrum (KBr) showed absorption at 3433 cm^{-1}, indicating the presence of hydroxyl groups supported by peak at 1050 cm^{-1} which represented C-O. Absorption at 2956, 2938, and 2869 cm-1 was from methyl and methylene, while 1634 cm^{-1} originated from C=C stretching, showing the presence of olefin groups, and C-H bending appeared at 1465 cm^{-1}.

The ^{1}H NMR spectrum showed the presence of 2 methyl groups with singlet multiplicity at δH 0.67 (3H,s) and 1.00 ppm (3H,s). There were 4 methyl groups with signals at δH 0.80 (3H, d, J= 6 .7) 0.82 (3H, d, J= 6.7), 0.83 (3H, t, J= 6.7), and 0.91 ppm (3H, t, J= 6.1). COZY spectrum analysis showed a 1H-1H environmental correlation between the proton signal at H 1.15 ppm (H-1) and H 1.84 ppm (H-2) with H 3.51 ppm (H-3), H 3.51 ppm (H-3) with H 14.2 ppm (H-4), and a proton signal on H 5.34 ppm (H-6) with (H-7). A significant correlation was observed between proton signal on H 1.98 ppm (H-7) and H 1.49 ppm (H-8), H 1.49 ppm (H-8) and H 0.91 ppm (H-9), H 1.48 (H-11) and H 2.00 ppm (H-12), as well as H 1.49 ppm (H-8) and H 0.98 (H-14). Furthermore, proton signal on H 1.58 ppm (H-15)

correlated with H 1.82 ppm (H-16), H 1.82 ppm (H-16) with H 1.07 ppm (H-17), H 1.07 ppm (H-17) with H 1.34 ppm (H-20). COZY spectrum analysis also showed a 1H -1H environmental correlation between the proton signal at H 1.34 ppm (H-20), H 1.98 ppm (H-22), and 1.14 ppm (H-23), H 1.14 ppm (H-23) and H 0.89 ppm (H-24), H 0.89 ppm (H-24) and H 1.23 ppm (H-28), as well as H 1.23 (H-28) and H 0.83 ppm (H-29). Proton signal at H 0.89 ppm (H-24) and H 1.65 ppm (H-25) also correlated with H 0.80 ppm (H-27), H 1.65 ppm (H-25), and H 0.82 ppm (H-26). Based on the spectroscopic data, it was concluded that the compound was β-sitosterol (Figure 1 (b)), with the chemical formula ($C_{29}H_{50}O$) presented in Table 1.

The study identified β-sitosterol as a white (clear) crystalline compound with a melting point of 138-139^{o}C, which is within the reported range for pure β-sitosterol. This melting point consistency suggests high purity and minimal impurities in the isolated compound. To confirm its molecular structure, infrared (IR) spectroscopy was employed, revealing key absorption peaks that correspond to specific functional groups. The broad absorption band at 3433 cm^{-1} was indicative of the hydroxyl (-OH) group, which is a distinguishing feature of sterols. This hydroxyl presence was further supported by a peak at 1050 cm^{-1}, representing the C-O stretching vibration, confirming the existence of an alcohol functional group in the molecular

Table 1. The result of ^{1}H-NMR and ^{13}C-NMR of β-Sitosterol compound.

No	^{1}H-NMR δH: ppm (multiplisitas, *J* dlm HZ)	δc (ppm)	HMBC
1	1.15 (2H, *dt, J*=11.0 ; 3. 65 Hz) 1.08 (1H,*m*)	37.3	5, 10, 9
2	1.84 (1H,*m*) 1.54 (1H,*m*)	31.7	3, 4
3	3.51 (1H,*m*)	140.8	-
4	2.28 (1H,*m*) 2.22 (1H,*m*)	42.4	3, 5
5	3.51 (1H,*m*)	71.9	-
6	5.34 (3H. *d, J*= 4.90 Hz)	121.8	7
7	1.98 (1H,*m*) 1.94 (1H, *m*)	32.0	8, 24
8	1.49 (1H,*m*)	32.0	8, 14
9	0. 91 (1H,*m*)	50.2	10
10	-	36.2	-
11	1.48 (2H, *m*)	21.2	8, 9, 12
12	2.00 (1H,*m*)	39.8	-
13	-	42.4	-
14	0.98 (1H,*m*)	56.8	8, 13
15	1.58 (1H,*m*)	24.4	8, 14
16	1.82 (1H,*m*)	28.4	-
17	1.07 (1H,*m*)	56.1	13, 16
18	0,67 (3H, s)	121.1	12, 13, 14, 17
19	1.00 (3H, s)	19.1	5, 9, 10
20	1.34 (1H,*m*)	36.6	-
21	0.91 (3H, *d, J*= 6.1Hz)	18.9	17, 20, 22
22	1.98 (1H,*m*)	34.0	27, 20, 23
23	1.14(2H, *m*)	26.1	-
24	0. 89	45.9	-
25	1.65 (1H,*m*)	29.2	24
26	0.82 (3H,*d, J*= 6.7Hz)	19.9	24, 25
27	0.80 (3H, *d, J*= 6.7Hz)	19.5	24, 25
28	1.23 (2H,*m*)	23.1	23, 24, 29
29	0.83 (3H,*t,J*= 6.7 Hz)	12.0	-

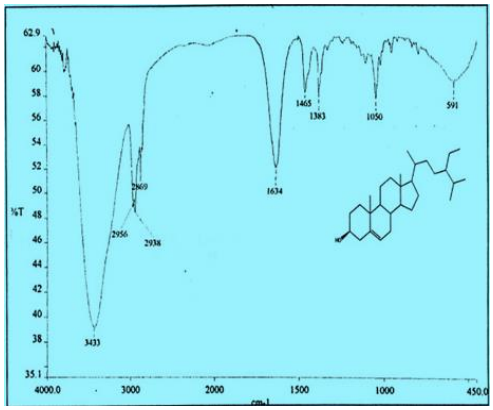

(a)

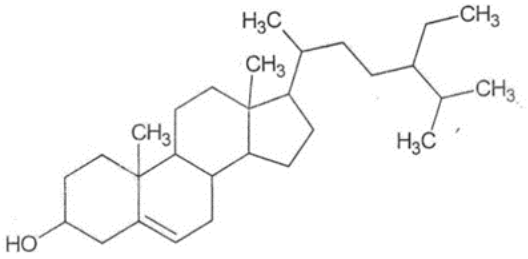

(b)

Figure 1. (a) The IR spectrum for β-sitosterol compound; (b) Chemical structure of β-sitosterol (Johannes, 2008).

structure. Additionally, multiple absorption bands at 2956, 2938, and 2869 cm^{-1} were assigned to the stretching vibrations of methyl ($-CH_3$) and methylene ($-CH_2$) groups, which are characteristic of the long aliphatic hydrocarbon chains present in β-sitosterol. Further structural confirmation was provided by the absorption peak at 1634 cm^{-1}, which was attributed to C=C stretching, indicating the presence of an olefinic (alkene) functional group within the sterol skeleton. This feature is consistent with the unsaturated sterol structure of β-sitosterol. Additionally, the peak at 1465 cm^{-1} was identified as C-H bending, which is commonly associated with aliphatic hydrocarbon frameworks. These spectral characteristics, in combination with the observed physical properties, provide strong evidence that the isolated compound is β-sitosterol. This confirmation is significant, as β-sitosterol is a well-known phytosterol with various pharmacological applications, including cholesterol-lowering effects, anti-inflammatory properties, and potential anticancer activity. The study's findings reinforce the accuracy of the identification process and validate the compound's structural integrity through multiple analytical techniques (Erdagi *et al*., 2022; Miya *et al*., 2023; Oladipupo *et al*., 2023; El-Ayouty *et al*., 2024).

The identification of β-sitosterol is based on the principles of IR and ^1H NMR spectroscopy, both of which provide valuable structural information by analyzing molecular vibrations and proton environments. Infrared (IR) spectroscopy involves the absorption of infrared radiation by molecular bonds, causing them to vibrate at specific frequencies. The broad absorption at 3433 cm^{-1} indicates the presence of a hydroxyl group (-OH), typical of alcohols, due to O-H stretching, which is often broadened by hydrogen bonding. The peak at 1050 cm^{-1} corresponds to C-O stretching, confirming the alcohol functionality. The peaks at 2956, 2938, and 2869 cm^{-1} are attributed to C-H stretching in methyl ($-CH_3$) and methylene ($-CH_2$) groups, which are part of the sterol's hydrocarbon backbone. The absorption at 1634 $cm^{-1}$is due to C=C stretching, confirming the presence of an unsaturated bond in the sterol ring system. Additionally, C-H bending at 1465 cm^{-1} suggests the presence of aliphatic groups, which are common in sterols. ^1H NMR spectroscopy provides detailed information about proton environments based on their chemical shifts (δH), which reflect the electronic environment around the protons. The singlet peaks at δH 0.67 and 1.00 ppm are indicative of non-coupled methyl groups. Additional methyl signals at δH 0.80, 0.82, 0.83, and 0.91 ppm show coupling patterns typical of sterol structures, with J-couplings suggesting the presence of adjacent hydrogens. The olefinic proton at δH 5.34 ppm confirms the C=C bond, characteristic of sterols. ^1H-^1H COSY correlations further support the connectivity between protons in the sterol ring and the aliphatic side chain, with couplings such as H-1 (1.15 ppm) with H-2 (1.84 ppm) and H-6 (5.34 ppm) with H-7 (1.98 ppm) confirming the sterol structure. These combined spectral features conclusively identify β-sitosterol as a hydroxylated sterol with a double bond and a long hydrocarbon chain (Miya *et al*., 2023; El-Ayouty *et al*., 2024; Shekwa, 2022; Alharbi *et al*., 2024).

Antimicrobial activity of β-sitosterol compound against Xanthomonas campestris InaCC B1449

The results of antibacterial activity of β-sitosterol against *X. campestris* InaCC B1449 are shown in Table 2. Antibacterial activity showed the largest average of inhibition zone diameter with 24 h incubation at a concentration of 60 ppm (21.55 mm), which increased to 22.30 mm at 48 h.

Table 2. Antimicrobial activity of β-sitosterol compound isolated from Hydroid *A. cupressina L.* against *Xanthomonas campestris* InaCC B1449.

Concentration	Average of Inhibition Zone Diameter (mm) *Xanthomonas campestris*	
	24 h	48 h
β-sitosterol 20 ppm	12.40[b]	15.50[b]
β-sitosterol 40 ppm	19.30[c]	20.40[d]
β-sitosterol 60 ppm	21.55[e]	22.30[e]
Ciprofloxacin (positive control)	20.30[d]	20.00[c]
Distilled water (negative control)	00.00[a]	00.00[a]

Table 3. The result of antifungal activity of β-sitosterol compound isolated from Hydroid *A. cupressina* L. against *Fusarium oxysporum* InaCC F641.

Concentration	Average of Inhibition Zone Diameter (mm) *Fusarium oxysporum*	
	48 h	72 h
β-sitosterol 20 ppm	11.20[b]	10.50[b]
β-sitosterol 40 ppm	18.30[c]	19.15[c]
β-sitosterol 60 ppm	20.43[e]	21.56[d]
Ketoconazole (positive control)	20.30[d]	21.50[d]
Distilled water (negative control)	00.00[a]	00.00[a]

Meanwhile, inhibition zone diameter formed at 24 h of incubation was 19.30 mm which increased to 20.40 mm at 40 ppm after 48 h. At a concentration of 20 ppm with an incubation period of 24 h, it was 12.40 mm and increased to 15.50 mm after 48 h. The positive control (ciprofloxacin) produced a higher inhibition zone diameter than the 20 and 40 ppm β-sitosterol concentrations but lower than the 60 ppm treatment. However, distilled water used as a negative control did not produce an inhibition zone diameter.

The antibacterial activity of β-sitosterol against *X. campestris* InaCC B1449 revealed a concentration-dependent and time-dependent pattern, with the highest efficacy observed at the 60 ppm concentration. After 24 h of incubation, the inhibition zone diameter at this concentration was 21.55 mm, and it increased slightly to 22.30 mm after 48 h, indicating that the antibacterial effect of β-sitosterol becomes more pronounced with extended exposure. This suggests that the compound exerts a cumulative antimicrobial effect, where prolonged incubation allows for more interaction between β-sitosterol and the bacterial cells, thereby enhancing its ability to inhibit bacterial growth. At 40 ppm, the inhibition zone was 19.30 mm after 24 h and 20.40 mm after 48 h, demonstrating a moderate antibacterial activity. The increase in inhibition zone size over time, although less pronounced than the 60 ppm treatment, still suggests that β-sitosterol has a dose-dependent effect. At 20 ppm, the inhibition zone at 24 h was smaller, measuring 12.40 mm, but it increased to 15.50 mm at 48 h, indicating that even at lower concentrations, β-sitosterol has the ability to inhibit bacterial growth, though its effectiveness is less compared to the higher concentrations. When compared to the positive control (ciprofloxacin), which is a synthetic antibiotic, β-sitosterol at 60 ppm showed a larger inhibition zone than the 20 ppm and 40 ppm concentrations, but it was smaller than the inhibition zone produced by ciprofloxacin. This indicates that β-sitosterol possesses strong antibacterial properties, although its activity is not as potent as the antibiotic. The negative control (distilled water) did not produce any inhibition zone, confirming that the observed antibacterial effects were due to the presence of β-sitosterol and not an experimental artifact. The results suggest that β-sitosterol can act as a natural antibacterial agent, with its effectiveness increasing at higher concentrations and longer exposure times, making it a promising candidate for further development as an antimicrobial compound (Anwar *et al*., 2022; Ibrahim and Abdul-Hafeez, 2023; Rossi *et al*., 2023; Reveglia *et al*., 2024).

Antifungal activity of β-sitosterol compound against Fusarium oxysporum InaCC F641

As presented in Table 3, β-sitosterol compound showed antifungal activity against *F. oxysporum* InaCC F641. The best inhibition zone diameter of 20.43 mm and 21.56 mm was obtained at a concentration of 60 ppm during 48 and 72 h of incubation, respectively. A concentration of 40 ppm showed inhibition zone diameter of 18.30 mm at 48 h of incubation and increased by 19.15 mm at 72 h. Meanwhile, the concentration of 20 ppm showed a decrease in the size of the inhibition zone diameter from 11.20 mm at 48 h to 10.50 mm at 72 h of

incubation. Concentrations of 60 and 40 ppm showed fungicidal activity against *F. oxysporum* InaCC F641. As a positive control, Ketoconazole showed 20.30 mm and 21.50 mm at 48 h and 72 h, respectively. However, the distilled water which served as negative control did not form an inhibition zone. The activity of β-sitosterol at 20 ppm against the fungus *F. oxysporum* InaCC F641 was fungistatic mechanism, characterized by a reduction in inhibition zone diameter after 72 h of incubation. The fungus cell wall was composed of chitin compounds, which only reacted with the structure outside the ring (CH_2-OH). Since there was no damage to the backbone structure of chitin, this compound did not kill the growth of fungus cells but only acted as an inhibitor (Merzendorfer and Cohen 2019). This was shown by β-sitosterol at concentrations of 40 ppm and 60 ppm, which are fungicidal because there was an increase in inhibition zone after 48 h and 72 h of incubation.

The antifungal activity of β-sitosterol against *F. oxysporum* InaCCF641 demonstrates both fungistatic and fungicidal effects, depending on the concentration and duration of exposure. At a concentration of 20 ppm, β-sitosterol displayed a reduction in the inhibition zone diameter from 11.20 mm after 48 h to 10.50 mm after 72 h. This reduction suggests that at this lower concentration, β-sitosterol acts in fungistatic manner, meaning it inhibits the growth of the fungus but does not kill the cells. The inhibition is reversible, as evidenced by the decrease in the inhibition zone over time, which is characteristic of a fungistatic compound. The fungistatic effect is likely due to β-sitosterol's interaction with the fungal cell wall, which is primarily composed of chitin. Chitin is a long-chain polymer of N-acetylglucosamine that provides structural support to the fungal cell. By inhibiting the synthesis or modification of chitin, β-sitosterol prevents the fungus from growing or proliferating, but it does not destroy the cell's structural integrity. This behavior aligns with findings from Merzendorfer and Cohen (2019), which highlighted that some compounds, including sterols like β-sitosterol, can inhibit fungal growth without causing damage to the fungal cell's backbone structure. The fungistatic activity of β-sitosterol at lower concentrations makes it a viable option for inhibiting fungal growth in environments where the goal is to stop further fungal proliferation rather than completely eradicate the organism. On the other hand, at higher concentrations (40 ppm and 60 ppm), β-sitosterol exhibited fungicidal activity, as demonstrated by the increasing inhibition zone diameters from 48 h to 72 h. At 40 ppm, the inhibition zone increased from 18.30 mm at 48 h to 19.15 mm at 72 h, and at 60 ppm, the inhibition zone grew from 20.43 mm at 48 h to 21.56 mm at 72 h, indicating a stronger, more lethal effect on the fungus over time. This increase in inhibition zone size over the incubation period is a characteristic feature of fungicidal activity, where the compound not only inhibits fungal growth but also actively kills the fungal cells. The increase in the inhibition zone diameter suggests that β-sitosterol at these higher concentrations has a profound effect on the fungal cell's integrity, potentially causing irreversible damage. The fungicidal mechanism of β-sitosterol is likely due to its ability to disrupt the fungal cell membrane, which consists of lipid bilayers and sterols. By interacting with these membrane components, β-sitosterol may alter the membrane's fluidity, leading to permeabilization. This disruption allows the leakage of vital cellular components, causing cell death. Additionally, β-sitosterol could induce oxidative stress, a known mechanism through which certain compounds damage cellular structures by generating reactive oxygen species (ROS). These ROS can damage lipids, proteins, and nucleic acids, leading to the complete breakdown of the fungal cell. The fungicidal properties of β-sitosterol at higher concentrations make it a potent antifungal agent capable of not only inhibiting fungal growth but also eradicating fungal cells, making it suitable for applications where fungal eradication is required. The dual nature of β-sitosterol, acting as both fungistatic and fungicidal depending on concentration, positions it as a versatile compound for future use in antifungal treatments, especially when tailored to specific needs in different environments (Udasi *et al*., 2023; Toka *et al*., 2023; Naqvi *et al*., 2023; Muwanya *et al*., 2024).

SEM morphology analysis of β-sitosterol effect against cell damage of Xanthomonas campestris InaCC B1449 and Fusarium oxysporum InaCC F641

The antibacterial and antifungal activity tests were 60 ppm β-sitosterol was used to observe the effect of these compounds on *X. campestri*s InaCC B1449 and *F. oxysporum* InaCC F641 using SEM. The results showed that the cell wall of the *X. campestri* InaCC B1449 was broken, as presented in Figure 2. Additionally, the cell wall of the fungus *F. oxysporum* InaCC F641 was damaged, leading to an irregular shape, as shown in Figure 3.

B-sitosterol damages fungal and bacterial cells by disrupting membrane integrity, as shown in SEM images. In fungal cells, key indicators of damage include cell wall disruption, visible as cracks or surface irregularities, suggesting interference with chitin and glucan. SEM images also reveal cell shrinkage and deformation, where cells appear collapsed due to loss of turgor pressure, indicating increased membrane permeability. Pore formation

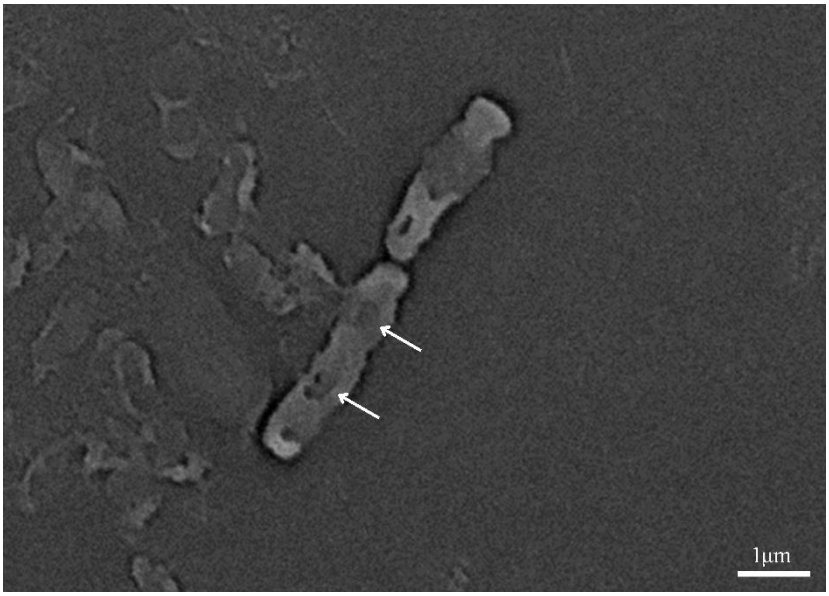

Figure 2. The result of SEM analysis of β-sitosterol effect against *X. campestri* InaCC B1449 (3000X magnification).

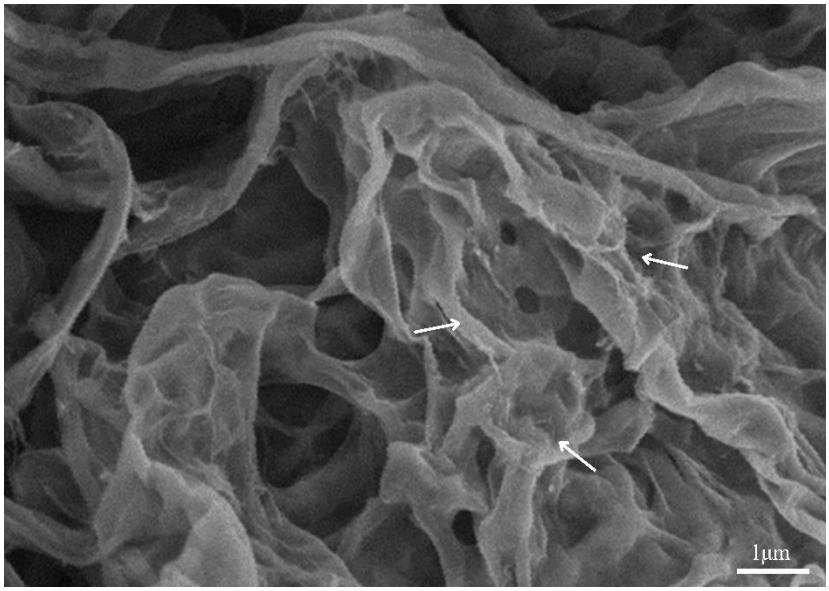

Figure 3. SEM analysis of β-sitosterol effect against *F. oxysporum* InaCC F641 (3000X magnification).

and cytoplasmic leakage are evident, as ruptured membranes release intracellular contents, leading to fungal lysis. In severe cases, aggregation of cellular debris is observed, marking complete structural breakdown. Similarly, bacterial cells exhibit irregular shape and surface roughness, with SEM images showing wrinkled textures, indicating compromised peptidoglycan layers. Another major sign is membrane blebbing and protrusions, where bulging structures emerge, reflecting stress-induced membrane instability. Some bacterial cells undergo fragmentation and lysis, as seen in ruptured membranes and dispersed cytoplasmic material, suggesting disrupted membrane potential and cell death. Additionally, bacterial cell aggregation is visible, likely due to altered membrane charge interactions. SEM images can highlight these damage markers with arrows, providing clear visual evidence of B-sitosterol's antimicrobial mechanism. Overall, B-sitosterol disrupts cell walls and membranes, leading to increased permeability, structural instability, and cell death. These findings support its potential as a natural antimicrobial agent, emphasizing the importance of SEM analysis

in understanding its effects on microbial cells (Saqib *et al*., 2022; Choudhary *et al*., 2022; Djearamane *et al*., 2022; Li *et al*., 2023).

Conclusion

This study identified β-sitosterol as a crystalline compound with significant antibacterial and antifungal activities. The IR and ^{1}H NMR spectra confirmed the presence of key functional groups such as hydroxyl, methyl, and olefinic bonds, characteristic of sterols. Antibacterial testing against *X. campestris* InaCC B1449 revealed a dose-dependent and time-dependent effect, with the largest inhibition zone of 21.55 mm at 60 ppm after 24 h, increasing to 22.30 mm after 48 h. At 40 ppm, the inhibition zone grew from 19.30 mm to 20.40 mm, and at 20 ppm, the inhibition zone expanded from 12.40 mm to 15.50 mm. In comparison, ciprofloxacin showed a larger inhibition zone than β-sitosterol at lower concentrations. Antifungal testing against *F. oxysporum* InaCC F641 showed fungistatic effects at 20 ppm and fungicidal effects at 40 ppm and 60 ppm, with the inhibition zone growing from 20.43 mm at 48 h to 21.56 mm at 72 h. These results demonstrate the potential of β-sitosterol as an effective antimicrobial agent.

References

Alharbi, H., Kahfi, J., Dutta, A., Jaremko, M., & Emwas, A.H. 2024. The detection of adulteration of olive oil with various vegetable oils–A case study using high-resolution 700 MHz NMR spectroscopy coupled with multivariate data analysis. *Food Control*, 166: p.110679. https://doi.org/10.1016/j.foodcont.2024.110679

Anwar, R., Sukmasari, S., Aisyah, S., & Ilfani, D. 2022. Antimicrobial Activity of β-Sitosterol Isolated from *Kalanchoe tomentosa* Leaves Against *Staphylococcus aureus* and *Klebsiella pneumonia*. *Pak. J. Biol. Sci.*, 25: 602-607. https://doi.org/10.3923/pjbs.2022.602.607

Chen, D., Zhong, X., Cui, J., Xie, J., & Kang, J. 2022. Comparative genomic analysis of *Xanthomonas campestris* pv. *campestris* isolates BJSJQ20200612 and GSXT20191014 provides novel insights into their genetic variability and virulence. *Front. Microbiol.*, 13: p.833318. https://doi.org/10.3389/fmicb.2022.833318

Choudhary, M., Verma, V., Saran, R., Bhagyawant, S.S., & Srivastava, N. 2022. Natural biosurfactant as antimicrobial agent: strategy to action against fungal and bacterial activities. *Cell. Biochem. Biophys.*, 80(1): 245-259. https://doi.org/10.1007/s12013-021-01045-1

De Lamo, F.J., & Takken, F.L. 2020. Biocontrol by *Fusarium oxysporum* using endophyte-mediated resistance. *Front. Plant. Sci.*, 11: p.500488. https://doi.org/10.3389/fpls.2020.00037

Djearamane, S., Xiu, L.J., Wong, L.S., Rajamani, R., Bharathi, D., Kayarohanam, S., De Cruz, A.E., Tey, L.H., Janakiraman, A.K., Aminuzzaman, M., & Selvaraj, S., 2022. Antifungal properties of zinc oxide nanoparticles on *Candida albicans*. *Coatings*, 2(12): p.1864. https://doi.org/10.3390/coatings12121864

El-Ayouty, M.M., Eltahawy, N.A., Abd El-Sameaa, A.M., Badawy, A.M., Darwish, K.M., Elhady, S.S., Shokr, M.M., & Ahmed, S.A. 2024. *In vivo* determination of analgesic and anti-inflammatory activities of isolated compounds from *Cleome amblyocarpa* and molecular modelling for the top active investigated compounds. *RSC Adv.*, 14(34): 24503-24515. https://doi.org/10.1039/D4RA04496G

Erdağı, S.İ. 2022. Design, Synthesis, and Biological Evaluation of Curcumin-β-sitosterol Conjugate a Potential Candidate for Breast Cancer Therapy. *Bilecik Seyh Edebali University J. Sci.*, 9(2): 866-880. https://doi.org/10.35193/bseufbd.1097 088

Gomathi, S., & Maneemegalai, S. 2024. Isolation, characterization of β-Sitosterol from the herbal extracts and evaluation of in vitro anti-oxidant and anti-diabetic activities. *J. Microbiol. Biotechnol. Food Sci.*, 13(4): 10236-10236. https://doi.org/10.55251/jmbfs.10236

Gwinn, K.D., Hansen, Z., Kelly, H., & Ownley, B.H. 2022. Diseases of *Cannabis sativa* caused by diverse Fusarium species. *Front. Agron.*, 3: p.796062. https://doi.org/10.3389/fagro.2021.796062

Hassan, H.A. 2020. Biology and Integrated Control of Tomato Wilt Caused by *Fusarium oxysporum* lycopersici: A Com-prehensive Review under the Light of Recent Advancements. *J. Bot. Res.*, 3(1): 84-99. https://doi.org/10.36959/771/564

Hassaan, M.A., & El Nemr, A. 2020. Pesticides pollution: Classifications, human health impact, extraction and treatment techniques. *Egypt J .Aquat. Res.*, 46(3): 207-220. https://doi.org/10.1016/j.ejar.2020.08.007

Ibrahim, O.H., & Abdul-Hafeez, E.Y. 2023. The acetone extract of *Albizia lebbeck* stem bark

and its in vitro cytotoxic and antimicrobial activities. *Horticult.*, 9(3): p.385. https://doi.org/10.33 90/horticulturae9030385

Johannes, E., Usman, H., & Ahmad, A. 2008. Isolasi, Karakterisasi, dan Uji Bioaktivitas Metabolit Sekunder dari Hydroid *Aglaophenia cupressina* Lamoureoux Sebagai Bahan Dasar Antimikroba. *J. Akta Kimia Indonesia*, 2(1): 1-10. https:// doi.org/10.20956/ica.v2i1.972

Johannes, E., Ishak, E., Usman, H., & Bilang, M. 2013. Effectiveness of extracted antibacterial compound from hydroid *Aglaophenia cupressina* Lamoureoux against bacterial cell of Escherichia coli. *Int. J. Sci. Technol. Res.,* 2(2): 138-43.

Khan, I.H., & Javaid, A. 2020. Antifungal activity and GC-MS analysis of n-butanol extract of quinoa (*Chenopodium quinoa* Willd.) leaves. *Bangladesh J. Bot.*, 49(4): 1045-1051. http://dx.doi.org/10.3329/bjb.v49i4.52537

Li, Y., Zhang, P., Li, M., Shakoor, N., Adeel, M., Zhou, P., Guo, M., Jiang, Y., Zhao, W., Lou, B., & Rui, Y. 2023. Application and mechanisms of metal-based nanoparticles in the control of bacterial and fungal crop diseases. *Pest. Manag. Sci.*, 79(1): 21-36. https://doi.org/10.1002/ps.7218

Luhata, L.P., & Usuki, T. 2021. Antibacterial activity of β-sitosterol isolated from the leaves of *Odontonema strictum* (*Acanthaceae*). *Bioorg. Med. Chem. Lett.*, 48: p.128248. https://doi.org/10.1016/j.bmcl.2021.128248

Merzendorfer, H., & Cohen, E. 2019. Chitin/chitosan: versatile ecological, industrial, and biomedical applications. *Extracellular Sugar-Based Biopolymers Matrices*, (12): 541-624. https://doi.org/10.1007/978-3-030-12919-4_14

Meena, P.D., Mehta, N., & Saharan, G.S. 2021. Minor pathogens: A worldwide challenge to cultivation of crucifers. *Agricult. Res. J.*, 58: 557–580. https://doi.org/10.5958/2395-146X.2021.00 081.8

Miya, G.M., Oriola, A.O., Payne, B., Cuyler, M., Lall, N., & Oyedeji, A.O. 2023. Steroids and Fatty Acid Esters from *Cyperus sexangularis* Leaf and Their Antioxidant, Anti-Inflammatory and Anti-Elastase Properties. *Molecules*, 28(8): 3434. https://doi. org/10.3390/molecules28083434

Moosavi, B., Liu, S., Wang, N.N., Zhu, X.L., & Yang, G.F. 2020. The anti-fungal β-sitosterol targets the yeast oxysterol-binding protein Osh4. *Pest. Manag. Sci.*, 76(2): 704-711. https://doi.org/10.1002/ps.5568

Morales-Cedeño, L.R., Del Carmen Orozco-Mosqueda, M., Loeza-Lara, P.D., Parra-Cota, F.I., De Los Santos-Villalobos, S., & Santoyo, G. 2021. Plant growth-promoting bacterial endophytes as biocontrol agents of pre-and post-harvest diseases: Fundamentals, methods of application and future perspectives. *Microbiol. Res.*, 242: p.126612. https://doi.org/10.1016/j.micres.2020.126612

Muwanya, L., Sibandze, G.F., Dludlu, M.N., & Simelane, S.B. 2024. Thin layer chromatography -direct bioautography guided isolation of β-sitosterol from the leaves of *Capparis fascicularis*. *Nat. Prod. Res.*, pp.1-6. https://doi.org/10.1080/14786419.2024.2345753

Naidu, R., Biswas, B., Willett, I.R., Cribb, J., Singh, B.K., Nathanail, C.P., Coulon, F., Semple, K.T., Jones, K.C., Barclay, A., & Aitken, R.J. 2021. Chemical pollution: A growing peril and potential catastrophic risk to humanity. *Environ. Int.*, 156: p.106616. https://doi.org/10.1016/j.envint.20 21.106616

Naqvi, S.F., Javaid, A., & Khan, I.H. 2023. Fungicidal activity of stem extract of *Chenopodium murale* L. against the pathogen of Fusarium wilt of tomato. *Allelopathy. J.*, 59(1):69-80. https://doi.org/10.26651/allelo.j/2023-59-1-1432

Oladipupo, A.R., Alaribe, S.C.A., Ogunlaja, A.S., Beniddir, M.A., Ogah, C.O., Okpuzor, J., & Coker, H.A. 2023. Chemical and Biological Insights on *Phaulopsis falcisepala*: A Source of Bioactive Compounds with Multifunctional Anticancer Potentials. *Chem. Afr.* 6(3): 1175-1189. https://doi.org/10.1007/s42250-022-00553-8

Rahim, S., Murshed, M., Umarbeyli, S., Kirikkaleli, D., Ahmad, M., Tufail, M., & Wahab, S. 2021. Do natural resources abundance and human capital development promote economic growth? A study on the resource curse hypothesis in Next Eleven countries. *Resour. Environ. Sustain.*, 4: p.100018. https://doi.org/10.1016/j.resenv.2 021.100018

Reveglia, P., Corso, G., & Evidente, A. 2024. Advances on Bioactive Metabolites with Potential for the Biocontrol of Plant Pathogenic Bacteria. *Pathogens*, 13(11): p.1000. https://doi.org/10.3390/pathogens13111000

Rossi, A., Bragonzi, A., Medede, M., De Fino, I., Lippi, G., Prosdocimi, M., Tamanini, A., Cabrini, G., &

Dechecchi, M.C. 2023. β-sitosterol ameliorates inflammation and *Pseudomonas aeruginosa* lung infection in a mouse model. *J. Cyst. Fibros.*, 22(1): 156-160. https://doi.org/10.1016/j.jcf.2022.08.005

Sampaio, A.M., Araujo, S.D., Rubiales, D., & Vaz Patto, M.C. 2020. Fusarium wilt management in legume crops. *Agronomy*, 10(8): p.1073. https://doi.org/10.3390/agronomy10081073

Saqib, S., Faryad, S., Afridi, M.I., Arshad, B., Younas, M., Naeem, M., Zaman, W., Ullah, F., Nisar, M., Ali, S., & Elgorban, A.M. 2022. Bimetallic assembled silver nanoparticles impregnated in *Aspergillus fumigatus* extract damage the bacterial membrane surface and release cellular contents. *Coatings*, 12(10): p.1505. https://doi.org/10.3390/coatings12101505

Shekwa, W. 2022. An investigation of antimicrobial compounds for dental health care from the leaf and stem extracts of *Carissa bispinosa* (L.) Desf ex Brenan (Apocynaceae). Dissertation. University of Limpopo. Polokwane. 159 pp.

Soleha, S., Muslim, A., Suwandi, S., Kadir, S., & Pratama, R. 2022. Host range studies of *Fusarium oxysporum*, causal agent of seedling wilt disease of *Acacia mangium*. *Biodiversitas*, 23(1): 25-32. https://doi.org/10.13057/biodiv/d230104

Steinberg, G., & Gurr, S.J. 2020. Fungi, fungicide discovery and global food security. *Fungal Genet .,* 144: p.103476. https://doi.org/10.1016/j.fgb.2020.103476

.

Toka, A.N., Ngatsi, P.Z., Dida, S.L.L., Tayo, P.M.T., Kuate, N.W.T., Boli, H., Atindo, T.S., Tize, T., & Ndongo, B. 2023. Phytochemical analysis and antifungal activity of *Azadirachta indica* and *Balanites aegyptiaca* seed extracts against *Fusarium oxysporum* isolate on tomatoes. *J. Glob. Innov. Agric. Sci.*, 11(3): 293-304. https://doi.org/10.22194/JGIAS/23.1159

Udasi, V., Shaikh, A., Urdukhe, Y., & Mogle, U. 2023. GCMS analysis and antifungal activity of leaf extracts of *Ailanthus excelsa* (Roxb), against *Fusarium oxysporum* causal agent of Fusarium wilt disease in tomato. *J Pharmacogn. Phytochem.*, 12(5): 428-432. https://doi.org/10.22271/phyto.2023.v12.i5e.14753

Ullah, S., Mostert, D., Serfontein, K., & Viljoen, A. 2021. The Survival and Treatment of *Fusarium oxysporum* f. sp. *cubense* in Water. *J. Fungi*, 7(10): p.796. https://doi.org/10.3390/jof7100796

Uttu, A.J., Sallau, M.S., Ibrahim, H., & Iyun, O.R.A. 2023. Isolation, characterization, and docking studies of campesterol and β-sitosterol from *Strychnos innocua* (Delile) root bark. *J. Taibah Univ. Med. Sci.*, 18(3): 566-578. https://doi.org/10.1016/j.jtumed.2022.12.003

Zubrod, J.P., Bundschuh, M., Arts, G., Brühl, C.A., Imfeld, G., Knäbel, A., Payraudeau, S., Rasmussen, J.J., Rohr, J., Scharmüller, A., & Smalling, K. 2019. Fungicides: an overlooked pesticide class?. *Environ. Sci. Technol.*, 53(7): 3347-3365. https://doi.org/10.1021/acs.est.8b04392